Modeling and Intelligent Power Flow Management of a High-Gain Three-Port Converter

Sreedevi S. Nair
Department of Electrical Engineering, Agnel Charities Fr. C. Rodrigues Institute of Technology, India
sreedevis.nair@fcrit.ac.in (corresponding author)

Mini Rajeev
Department of Electrical Engineering, Agnel Charities Fr. C. Rodrigues Institute of Technology, India
mini.rajeev@fcrit.ac.in

Received: 15 May 2025 | Revised: 22 June 2025 and 7 July 2025 | Accepted: 11 July 2025

 DOI: https://doi.org/10.48084/etasr.12159

ABSTRACT

The Three-port converter is an electronic power interface that enables simultaneous energy exchange among multiple energy sources and loads. This paper presents the modeling and intelligent control of a High Gain Boost Three-Port Converter (HGBTPC) for dynamic power flow management between the three ports. HGBTPC integrates Photovoltaic (PV) and battery sources to ensure a reliable power supply under varying conditions of source and load. A detailed state-space model of the HGBTPC was developed to capture the converter's dynamic behavior. In addition, a regression neural network was trained with inputs such as PV power, battery State of Charge (SOC), and load demand to predict optimal operating modes in real time. Key validation metrics, such as a confusion matrix, training vs loss accuracy, and mode transition tracking, confirm the effectiveness of the proposed model and the control scheme.

Keywords-PV; three-port converter; state-space modeling; deep neural network; power flow management

I. INTRODUCTION

Three-Port Converters (TPCs) are commonly used in systems involving multiple inputs, energy storage, and loads. Typical applications of TPCs are off-grid/on-grid systems, integration of renewable sources, Electric Vehicles (EVs), uninterrupted power supplies, microgrids, smart grids, IoT-powered systems, portable systems, drones, etc. [1]. TPCs with high voltage gain are gaining popularity because of better thermal performance and component stress reduction, while boosting the voltage levels. Key advantages of TPCs include:

- Improved efficiency and reliability due to the reduction in the number of components and power conversion stages.
- Integrated power management as a single converter handles the power flow between ports.
- Compactness, ideal for space-constrained applications.

Buck, boost, and buck-boost converters serve as the foundation for non-isolated TPCs in the literature [2]. Voltage multiplier cells have been used to increase voltage gain [3]. However, this leads to losses because there are many passive components. In [4], a TPC was considered, which provided comparable gain and efficiency without any voltage multiplier cells. TPC modeling allows virtual testing of various operating conditions, which may be impractical or hazardous to replicate on hardware. Researchers perform state-space modeling of various new topologies of boost converters to identify a controller that provides the desired output voltage [5].

Making decisions in real time to regulate the amount and direction of power flow among the three ports is known as power flow management in TPC. Dynamic operating conditions are changes in load demand, solar irradiance, temperature, and battery State-Of-Charge (SOC). Traditional rule-based control strategies may not perform optimally under nonlinear conditions, when objectives such as efficiency, battery life, and energy balance must be met simultaneously.

In [6], a multiport DC-DC converter was equipped with an Artificial Neural Network (ANN) controller for DC micro-grid applications. This combination offered adaptability, enabling intelligent decision-making in response to dynamic micro-grid conditions. In [7], a hybrid solar and wind grid-tied inverter system was controlled by a fuzzy controller based on an adaptive network. According to the simulation findings, the performance of the controller was superior to that of the conventional PI controller. In [8], an improved whale optimization algorithm was used to solve the dynamic optimal power flow problem in green energy systems. Fuzzy logic control enhanced the convergence performance of the entire system.

Artificial Neural Networks (ANNs) have emerged as a promising solution for intelligent power flow management in TPCs [9]. By training on historical data, ANNs can predict the most suitable power flow configuration. In [10-11], a real-time ANN-based power flow management for microgrids demonstrated effective energy control under varying conditions. In [12], an energy management approach was proposed for hybrid electric vehicles, using deep reinforcement learning and enabling efficient operation in varying driving conditions.

This study models a high-gain boost converter using state space modeling and validates the model through simulation. Furthermore, DNN-driven power flow management was implemented using a neural network-based prediction block in MATLAB/Simulink. The novelty of this work is as follows:

- Performs a seamless integration of a trained regression neural network into Simulink's real-time environment to eliminate the need for additional code generation or interfacing.
- Achieves multi-parameter decision-making.
- The proposed approach was applied to a high-gain TPC presented in [4].

II. MODELING OF HIGH GAIN TPC

Figure 1 shows the general configuration of the TPC. The state-space modeling of HGBTPC is presented in [4]. It has two inputs, solar and battery (V_{PV} and V_B) and a single output port (V_o). Design details and various operating modes are given in [4]. The state variables considered are i_{L1}, i_{L2}, V_{C1} and V_{co}. i_{L1} is the current through inductor L_1, i_{L2} is the current through inductor L_2, V_{C1} is the voltage across the intermediate capacitor C_1, and V_{co} is the voltage across the output capacitor C_o. Each of the four operating modes has its own set of matrices based on switch configuration and circuit topology. The model was simulated in MATLAB to validate its operating modes and its performance in Continuous Conduction Mode (CCM). In CCM, inductor currents (i_{L_1}, i_{L_2}) never fall to zero, ensuring continuous energy transfer and avoiding mode switching complexity. The terminology of ideal switches indicate zero ON resistance and infinite OFF resistance that provide instantaneous switching.

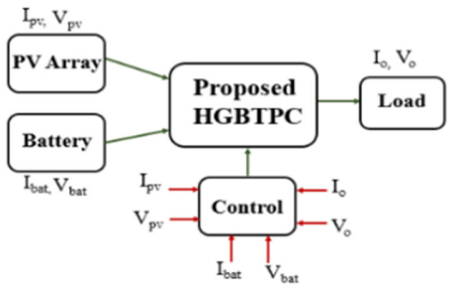

Fig. 1. General configuration of TPC.

A. *Operating Mode I: SISO$_{PV}$ Mode*

PV powers the load in this mode. S_B is ON, while S_C and S_D are OFF. The equations for state I and II when S_B is ON and OFF are shown in (1) and (2) from Figure 2(a, b). The state-space expressions are shown in (3, 4), respectively.

$$\frac{di_{L1}}{dt} = \frac{V_{PV}}{L_1} \; ; \quad \frac{di_{L2}}{dt} = \frac{(V_{PV}+V_{C1})}{L_2} \tag{1}$$

$$-i_{C1} = i_{L2}, \; i_{CO} = V_{C_o}/R \tag{2}$$

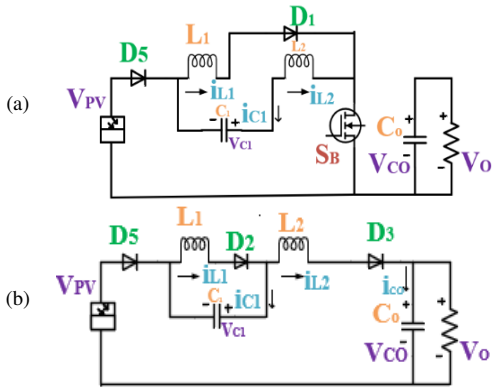

Fig. 2. (a) SISO$_{PV}$ mode in State I, (b) SISO$_{PV}$ mode in State II..

Similarly, when S_B is OFF, the equations and the state-space equations are as shown in (5), (6), and (7), respectively.

$$\begin{Bmatrix} \frac{di_{L1}}{dt} \\ \frac{di_{L2}}{dt} \\ \frac{dv_{C1}}{dt} \\ \frac{dv_{Co}}{dt} \end{Bmatrix} = \begin{Bmatrix} 0 & 0 & 0 & 0 \\ 0 & 0 & \frac{1}{L2} & 0 \\ 0 & -1/C1 & 0 & 0 \\ 0 & 0 & 0 & -1/RC_O \end{Bmatrix} \begin{Bmatrix} i_{L1} \\ i_{L2} \\ v_{C1} \\ v_{CO} \end{Bmatrix} + \begin{Bmatrix} 1/L1 & 0 \\ 1/L2 & 0 \\ 0 & 0 \\ 0 & 0 \end{Bmatrix} \begin{Bmatrix} V_{PV} \\ V_B \end{Bmatrix} \tag{3}$$

$$V_O = \{0\,0\,0\,1\} \begin{Bmatrix} i_{L1} \\ i_{L2} \\ v_{C1} \\ v_{CO} \end{Bmatrix} + \begin{Bmatrix} 0 & 0 \\ 0 & 0 \\ 0 & 0 \\ 0 & 0 \end{Bmatrix} \begin{Bmatrix} V_{PV} \\ V_B \end{Bmatrix} \tag{4}$$

$$\frac{di_{L1}}{dt} = -\frac{V_{C1}}{L_1} \; ; \frac{di_{L2}}{dt} = -\frac{(V_O - V_{PV} - V_{C1})}{L_2} \tag{5}$$

$$i_{C1} = i_{L1} \qquad i_{Co} = i_{L2} - i_o \tag{6}$$

$$\begin{Bmatrix} \frac{di_{L1}}{dt} \\ \frac{di_{L2}}{dt} \\ \frac{dv_{C1}}{dt} \\ \frac{dv_{Co}}{dt} \end{Bmatrix} = \begin{Bmatrix} 0 & 0 & -\frac{1}{L1} & 0 \\ 0 & 0 & \frac{1}{L2} & -1/L2 \\ 1/C1 & 0 & 0 & 0 \\ 0 & 1/C_O & 0 & -1/RC_O \end{Bmatrix} \begin{Bmatrix} i_{L1} \\ i_{L2} \\ v_{C1} \\ v_{CO} \end{Bmatrix} + \begin{Bmatrix} 0 & 0 \\ 1/L_2 & 0 \\ 0 & 0 \\ 0 & 0 \end{Bmatrix} \begin{Bmatrix} V_{PV} \\ V_B \end{Bmatrix} \tag{7}$$

The output voltage expression in (4) remains the same for all the operating modes.

B. Operating Mode II: SISO$_{BAT}$ Mode

During nighttime, PV is unavailable, hence the battery is the only source. Figure 3 shows the equivalent circuit. The operation resembles the SISO$_{PV}$ mode, with two operating states corresponding to the ON and OFF conditions of switch S_B. S_D is continuously ON. Assuming the battery is fully charged, the equations for both the states and the state space expressions are shown in (8-13).

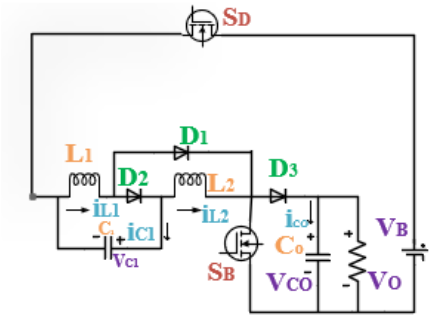

Fig. 3. SISO$_{BAT}$ mode (full equivalent circuit).

$$\frac{di_{L1}}{dt} = \frac{V_B}{L_1}; \quad \frac{di_{L2}}{dt} = \frac{(V_B + V_{C1})}{L_2} \tag{8}$$

$$-i_{C1} = i_{L2}; \quad i_{CO=} -V_{Co}/R \tag{9}$$

$$\frac{di_{L1}}{dt} = -\frac{V_{C1}}{L_1}; \quad \frac{di_{L2}}{dt} = -\frac{(V_O - V_B - V_{C1})}{L_2} \tag{10}$$

$$i_{C1} = i_{L1} \tag{11}$$

$$\begin{Bmatrix} \frac{di_{L1}}{dt} \\ \frac{di_{L2}}{dt} \\ \frac{dv_{C1}}{dt} \\ \frac{dv_{Co}}{dt} \end{Bmatrix} = \begin{Bmatrix} 0 & 0 & 0 & 0 \\ 0 & 0 & \frac{1}{L2} & 0 \\ 0 & -1/C1 & 0 & 0 \\ 0 & 0 & 0 & -1/RC_O \end{Bmatrix} \begin{Bmatrix} i_{L1} \\ i_{L2} \\ v_{C1} \\ v_{CO} \end{Bmatrix} + \begin{Bmatrix} 0 & 1/L_1 \\ 0 & 1/L_2 \\ 0 & 0 \\ 0 & 0 \end{Bmatrix} \begin{Bmatrix} V_{PV} \\ V_B \end{Bmatrix} \tag{12}$$

$$\begin{Bmatrix} \frac{di_{L1}}{dt} \\ \frac{di_{L2}}{dt} \\ \frac{dv_{C1}}{dt} \\ \frac{dv_{Co}}{dt} \end{Bmatrix} = \begin{Bmatrix} 0 & 0 & -\frac{1}{L1} & 0 \\ 0 & 0 & \frac{1}{L2} & -1/L2 \\ 1/C1 & 0 & 0 & 0 \\ 0 & 1/C_O & 0 & -1/RC_O \end{Bmatrix} \begin{Bmatrix} i_{L1} \\ i_{L2} \\ v_{C1} \\ v_{CO} \end{Bmatrix} + \begin{Bmatrix} 0 & 0 \\ 0 & 1/L_2 \\ 0 & 0 \\ 0 & 0 \end{Bmatrix} \begin{Bmatrix} V_{PV} \\ V_B \end{Bmatrix} \tag{13}$$

C. Operating Mode III: DISO Mode

When the PV cannot fulfill the load demand, the battery will again be active. In DISO mode, S_B and S_D are ON, and S_C remains OFF, as in Figure 4. The equations and the expressions governing the state space model of the second and the third operating states are given in (14-17).

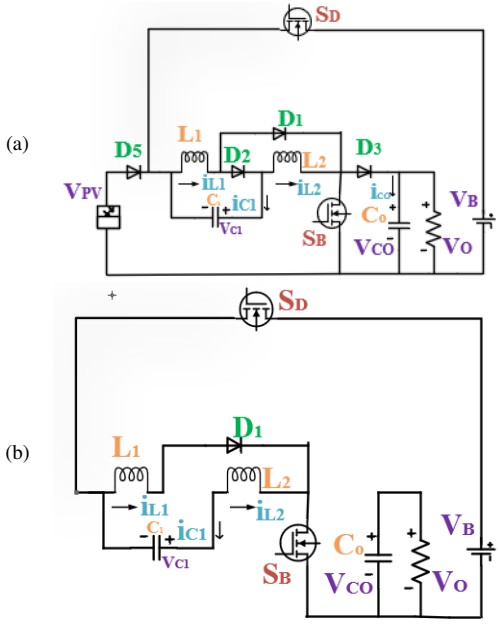

Fig. 4. (a) DISO mode (full equivalent circuit), (b) State II of DISO mode.

$$\frac{di_{L1}}{dt} = \frac{V_B}{L_1}; \quad \frac{di_{L2}}{dt} = \frac{(V_B + V_{C1})}{L_2} \tag{14}$$

$$\frac{di_{L1}}{dt} = -\frac{V_{C1}}{L_1}; \quad \frac{di_{L2}}{dt} = -\frac{(V_O - V_B - V_{C1})}{L_2} \tag{15}$$

$$\begin{Bmatrix} \frac{di_{L1}}{dt} \\ \frac{di_{L2}}{dt} \\ \frac{dv_{C1}}{dt} \\ \frac{dv_{Co}}{dt} \end{Bmatrix} = \begin{Bmatrix} 0 & 0 & 0 & 0 \\ 0 & 0 & \frac{1}{L2} & 0 \\ 0 & -1/C1 & 0 & 0 \\ 0 & 0 & 0 & -1/RC_O \end{Bmatrix} \begin{Bmatrix} i_{L1} \\ i_{L2} \\ v_{C1} \\ v_{CO} \end{Bmatrix} + \begin{Bmatrix} 0 & 0 \\ 0 & 1/L_2 \\ 0 & 0 \\ 0 & 0 \end{Bmatrix} \begin{Bmatrix} V_{PV} \\ V_B \end{Bmatrix} \tag{16}$$

$$\begin{Bmatrix} \frac{di_{L1}}{dt} \\ \frac{di_{L2}}{dt} \\ \frac{dv_{C1}}{dt} \\ \frac{dv_{Co}}{dt} \end{Bmatrix} = \begin{Bmatrix} 0 & 0 & -\frac{1}{L1} & 0 \\ 0 & 0 & \frac{1}{L2} & -1/L2 \\ 1/C1 & 0 & 0 & 0 \\ 0 & 1/C_O & 0 & -1/RC_O \end{Bmatrix} \begin{Bmatrix} i_{L1} \\ i_{L2} \\ v_{C1} \\ v_{CO} \end{Bmatrix} + \begin{Bmatrix} 0 & 0 \\ 0 & 1/L_2 \\ 0 & 0 \\ 0 & 0 \end{Bmatrix} \begin{Bmatrix} V_{PV} \\ V_B \end{Bmatrix} \tag{17}$$

D. Operating Mode III: SIDO Mode

The converter operates in SIDO mode as illustrated in Figure 5. Switch S_D remains OFF, while switches S_B and S_C actively regulate both load power and the battery voltage. The SIDO mode consists of three distinct operating states. The first and last states are State I and State II of the $SISO_{PV}$ mode. The equations and state space of state II are given in (18-20).

$$V_B = V_{PV} - V_{L1} \quad (18)$$

$$V_O = V_{PV} + V_{C1} - V_{L2} \quad (19)$$

$$\begin{Bmatrix} \frac{di_{L1}}{dt} \\ \frac{di_{L2}}{dt} \\ \frac{dv_{C1}}{dt} \\ \frac{dv_{Co}}{dt} \end{Bmatrix} = \begin{Bmatrix} 0 & 0 & -\frac{1}{L1} & 0 \\ 0 & 0 & \frac{1}{L2} & -1/L2 \\ 1/C1 & 0 & 0 & 0 \\ 0 & 1/C_O & 0 & -1/RC_O \end{Bmatrix} \begin{Bmatrix} i_{L1} \\ i_{L2} \\ v_{C1} \\ v_{CO} \end{Bmatrix} + \begin{Bmatrix} 1/L_1 & -1/L_2 \\ 0 & 1/L_2 \\ 0 & 0 \\ 0 & 0 \end{Bmatrix} \begin{Bmatrix} V_{PV} \\ V_B \end{Bmatrix} \quad (20)$$

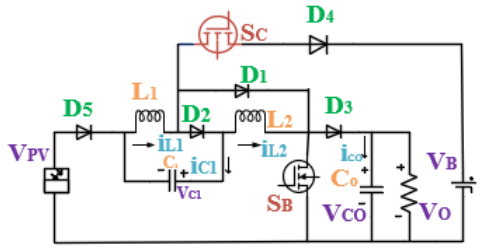

Fig. 5. SIDO mode (full equivalent circuit).

III. SIMULATION RESULTS AND ANALYSIS

The $SISO_{PV}$ mode was simulated using the averaged state-space model derived in Section II. The simulation was performed in MATLAB/Simulink, and Table I shows the simulation parameters.

TABLE I. SIMULATION PARAMETERS

Parameters	Specifications
Input Voltages (V_{PV}, V_B)	24V, 24V
Inductors (L_1 and L_2)	50µH, 225µH
Switching frequency (f_s)	20kHz
Capacitors (C_o, C_1)	100µF, 120µF
Output Voltage (V_o)	120V
Output Power (P_o)	200W

The results in Figure 6 illustrate the waveforms of all four state variables in $SISO_{PV}$ mode. The results confirm that the converter achieves a stable output voltage of 120V, which is the same as the capacitor voltage V_{CO}. The inductor currents exhibit a low ripple of 1 A and 0.2 A, which is in line with the design specifications. The capacitor voltages remain within the safe operating limits, validating the effectiveness of the $SISO_{PV}$ mode under the defined load conditions.

Modeling helps to assess the impact of parasitic elements, such as inductor Equivalent Series Resistance (ESR), on system efficiency for varying load conditions. The ESR of inductor L_1 is r_{l1} and the ESR of inductor L_2 is r_{l2}. A high inductor ESR value contributes to voltage drops, thus affecting voltage regulation. Figure 7 shows the simulation results considering the ESR of both inductors. It can be seen that efficiency drops while considering the ESR of both inductors. A high value of capacitor ESR increases output voltage ripple due to the voltage drop across the ESR during capacitor charging and discharging. This will reduce voltages V_{C1} and V_{CO}. Also, power dissipation will be within the capacitor, reducing efficiency. Considering the equivalent series ESR of both inductors of TPC, it is observed that the system achieves peak efficiency at an output power level of approximately 200 W, as shown in Figure 7. Consequently, this power level was selected as the reference point for training the ANN.

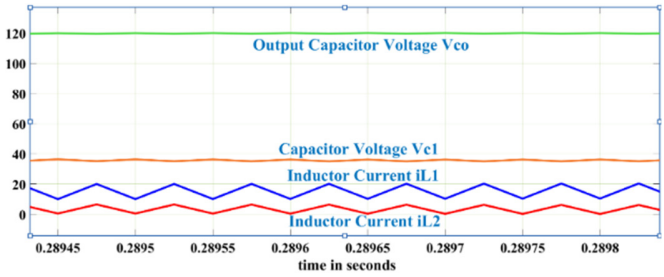

Fig. 6. Waveform of state variables.

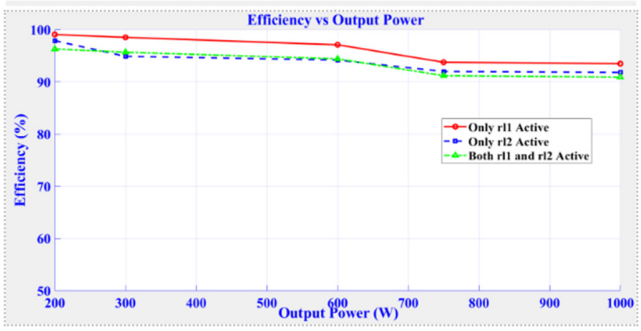

Fig. 7. Efficiency vs output power.

IV. POWER FLOW MANAGEMENT USING DNN

ANNs offer an adaptive and flexible approach in handling the characteristics of multi-input, multi-output power converters. Deep learning-based strategies for optimal scheduling, energy management, and intelligent control in microgrids and grid-connected renewable energy systems have been presented in [13-15]. This work uses a DNN-based controller using MATLAB's Regression Neural Network Predict block to intelligently manage the power flow in HGBTPC. The intelligent power management system takes real-time input and outputs a scalar value corresponding to one of the operating modes according to the power flow management algorithm depicted in Figure 8 [16].

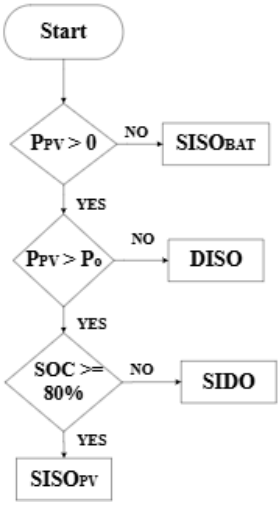

Fig. 8. Power flow management algorithm.

A. ANN Architecture and Training Strategy

The ANN architecture consists of an input layer, a hidden layer, and an output layer. The input layer receives three features: PV power, SOC of battery, and load power. A single hidden-layer neural network comprising 10 neurons was selected, which ensures a low training time and a reduced risk of overfitting while maintaining acceptable prediction accuracy. The Rectified Linear Unit (ReLU) activation function improves training convergence speed and is computationally efficient for real-time applications. A SoftMax function is used in the output layer to convert raw output scores into probability distributions, ensuring that the output probabilities sum to 1, making interpretation easier. The output layer corresponds to the four operating modes of HGBTPC.

A hold-out validation method was employed, where the available dataset was divided into three non-overlapping subsets: a training set comprising 70% of the total data, a validation set comprising approximately 15% of the dataset, and a test set comprising the remaining 15% of the data. The dataset is generated by simulating a two-input quadratic boost converter under varying solar irradiance, load power, battery current, and SOC conditions. The power flow mode for each data point was labeled based on predefined operational criteria. Early stopping was employed to prevent overfitting, where training was monitored using the validation loss. The training stopped if the validation loss did not improve over a specified number of epochs. The Adam optimizer was employed, with a mini-batch size of 64 samples [17]. Training was carried out for a maximum of 100 epochs. The training loss curve indicates the error reduction over training epochs. The gradual decrease in loss shows that the model is improving with each epoch, indicating effective learning during training, as shown in Figure 9.

Figure 10 shows the confusion matrix for the results. The model accurately predicted 996 out of 1000 $SISO_{PV}$ samples, with only four misclassified as DISO, yielding a class-specific accuracy of 99.6%. $SISO_{BAT}$ was classified with 100% accuracy, indicating the network's robustness in recognizing battery-only operation. For SIDO mode, 981 instances were correctly classified, with 19 misclassified as $SISO_{PV}$, resulting in an accuracy of 98.1%. DISO mode achieved 98.4% accuracy, with 16 samples misclassified as $SISO_{BAT}$. High diagonal accuracy (>95%) for all classes demonstrates the strong learning ability of the model.

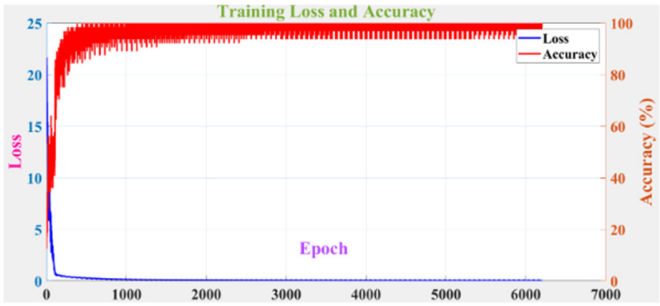

Fig. 9. Training loss vs. accuracy.

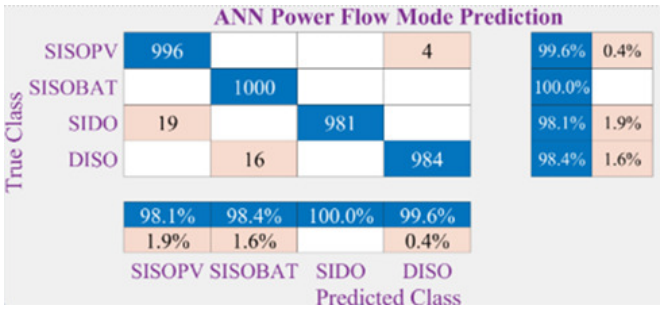

Fig. 10. Confusion matrix.

B. Precision, Recall, and F1-score

Precision and recall are two essential measures for assessing the effectiveness of classification models in neural networks. The precision of the model indicates its ability to accurately identify the positive cases out of all the instances that were expected to be positive, focusing on how accurate the optimistic forecasts were. Recall gauges the model's capacity to identify every real positive event, whereas the F1-score computes the harmonic mean of precision and recall to integrate them into a single value. The metrics range from 0 to 1. Figure 11 shows that all three metrics have a value near to 1, which signifies ideal classification performance.

classNames	precision	recall	f1score
{'SISOPV' }	0.94877	1	0.97371
{'SISOBAT'}	0.97847	1	0.98912
{'SIDO' }	1	0.949	0.97383
{'DISO' }	1	0.975	0.98734

Fig. 11. Precision, recall, and F1-score.

V. RESULTS AND DISCUSSION

The trained neural network was integrated with the HGBTPC model to control the three switches S_C, S_B, and S_D.

The model was run in Simulink. The outcome is an integer that indicates any of the four operational modes. This integer value is inputted into the control logic, which generates the correct pulses for each operating mode. The model was validated under dynamic conditions by varying the PV power and battery SOC. The PV power was initially set at 265 W and subsequently reduced to 230 W, 0 W, and finally 150 W with a time gap of 0.1 s. Simultaneously, the battery SOC varied from 54% to 86% as shown in Figure 12. Load power was kept at 200W. S_B was ON for all the modes; hence, the transition of the other two switches is shown in the figure. The following observations were noted:

- When PV is 265 W and the battery SOC is 54%, the system prioritizes to SIDO mode till $t = 0.1$ s. S_C and S_B are ON and S_D is OFF, indicating that the battery is getting charged.
- As PV power reduced to 230 W and the battery SOC was 86%, the system switched to $SISO_{PV}$ mode from $t = 0.1$ s to $t = 0.2$ s. Only S_B is ON. S_C and S_D are OFF, indicating that the PV is adequate to feed the load.
- When the PV power becomes 0 W, the system autonomously shifts towards battery-supported mode ($SISO_{BAT}$ mode), where S_C is OFF and S_D is ON.
- When PV resumes at 150 W, DISO is selected to optimally share the power between PV and battery. Only S_B and S_D are ON in this mode.

These results confirm that the ANN-based controller dynamically manages mode transitions accurately. In all the operating modes, the load voltage is maintained at 120 V. The smooth transitions and accurate pulse generation validate the practical feasibility and robustness of the proposed control scheme for hybrid energy systems.

A comparative analysis was conducted against the Fuzzy Logic Controller (FLC) and Rule-Based Logic (RBL) to validate the proposed intelligent power flow controller. The theoretical performance of these controllers is documented in [18-22]. Table II summarizes the comparative performance characteristics of these methods. The strengths of the proposed DNN-based method are real-time adaptability, improved efficiency, and system stability, which contribute to improved battery life and smoother transitions between operating modes. However, if the dataset lacks diversity and does not encompass a wide range of operating conditions, the model may not be able to generalize effectively, leading to overfitting and reduced reliability in practical applications.

TABLE II. COMPARATIVE PERFORMANCE

Metric	DNN	FLC [18-19]	RBL [20-21]
Mode-switch delay (ms)	5	40–60	30–50
Prediction accuracy (%)	98.5	85–90	75–85
Dynamic Response	High	Medium	Low
Rule/membership tuning	None (trained)	Required	Manual

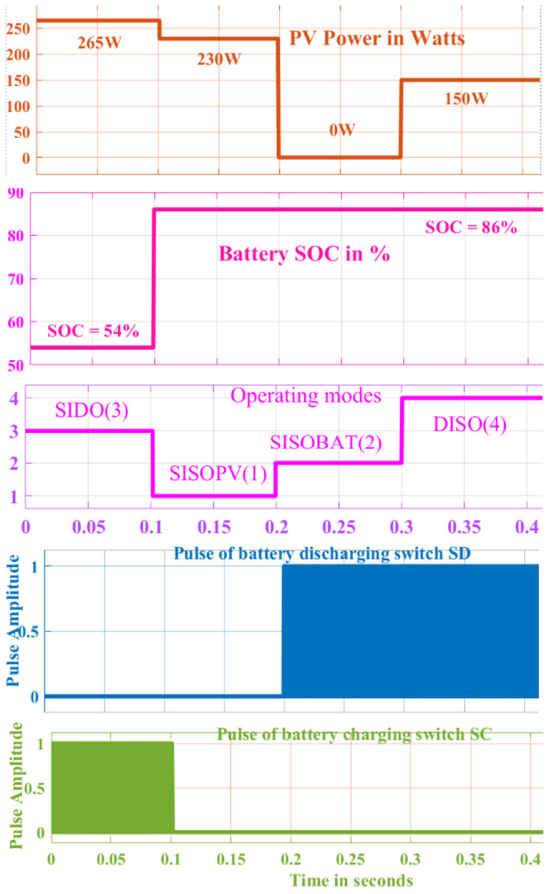

Fig. 12. Power flow management using ANN.

VI. CONCLUSION

This study developed and analyzed a model of the proposed converter [4]. The analysis reveals that the converter achieves maximum efficiency at a power level of 200 W. Accordingly, a regression neural network was trained at this optimal operating point to enable real-time prediction of the operating modes of HGBTPC. The simulation results demonstrated that the ANN facilitates intelligent decision-making, validating its effectiveness for real-time power flow management. In smart grid architectures, energy resources such as solar PV, wind turbines, and distributed batteries must be coordinated efficiently to ensure grid stability and energy reliability. In EVs, a DNN-based management strategy can support intelligent charging and battery life preservation, enabling Vehicle-to-Grid (V2G) and Vehicle-to-Home (V2H) operation with real-time grid condition awareness.

A practical implication of using DNNs in modern energy systems is their ability to efficiently manage power flow by making rapid and precise real-time decisions. Future work should focus on implementing the trained DNN model on real-time platforms using DSP processors, which is already in progress. Deeper architectures, such as Convolutional Neural Networks (CNNs), Long Short-Term Memory (LSTM) networks, or hybrid models, can also be explored to capture temporal dependencies and nonlinear correlations more effectively in dynamic power systems.

REFERENCES

[1] N. Zhang, D. Sutanto, and K. M. Muttaqi, "A review of topologies of three-port DC–DC converters for the integration of renewable energy and energy storage system," *Renewable and Sustainable Energy Reviews*, vol. 56, pp. 388–401, Apr. 2016, https://doi.org/10.1016/j.rser.2015.11.079.

[2] A. Nahavandi, M. T. Hagh, M. B. B. Sharifian, and S. Danyali, "A nonisolated multiinput multioutput DC–DC boost converter for electric vehicle applications," *IEEE Transactions on Power Electronics*, vol. 30, no. 4, pp. 1818–1835, Apr. 2015, https://doi.org/10.1109/TPEL.2014.2325830.

[3] V. A. K. Prabhala, P. Fajri, V. S. P. Gouribhatla, B. P. Baddipadiga, and M. Ferdowsi, "A DC–DC Converter With High Voltage Gain and Two Input Boost Stages," *IEEE Transactions on Power Electronics*, vol. 31, no. 6, pp. 4206–4215, Jun. 2016, https://doi.org/10.1109/TPEL.2015.2476377.

[4] S. S. Nair and M. Rajeev, "A Novel High Gain Non-Isolated Three-port Converter for Stand-Alone PV Applications," in *2023 International Conference on Computer, Electronics & Electrical Engineering & their Applications (IC2E3)*, Srinagar Garhwal, India, Jun. 2023, pp. 1–6, https://doi.org/10.1109/IC2E357697.2023.10262587.

[5] M. T. Zaman, X. Fu, and R. Challoo, "State-Space Average Modeling Based PID Control for Three Novel Topologies of DC-DC Boost Converter," in *2022 IEEE International Women in Engineering (WIE) Conference on Electrical and Computer Engineering (WIECON-ECE)*, Naya Raipur, India, Dec. 2022, pp. 115–120, https://doi.org/10.1109/WIECON-ECE57977.2022.10150510.

[6] P. Gopi, S. V. Rao, G. V. Reddy, and B. V. V. Reddy, "A multiport DC-DC converter with an intelligent controller for micro grid applications," in *Integrated Technologies in Electrical, Electronics and Biotechnology Engineering*, CRC Press, 2025.

[7] D. N. Truong, V. T. Ngo, M. S. N. Thi, and A. Q. Hoang, "Application of an Adaptive Network-based Fuzzy Inference System to Control a Hybrid Solar and Wind Grid-Tie Inverter," *Engineering, Technology & Applied Science Research*, vol. 11, no. 5, pp. 7673–7677, Oct. 2021, https://doi.org/10.48084/etasr.4413.

[8] K. Widarsono, A. Soeprijanto, and R. S. Wibowo, "Improved Whale Optimization Algorithm for Dynamic Optimal Power Flow with Renewable Energy Penetration," *Engineering, Technology & Applied Science Research*, vol. 15, no. 1, pp. 20379–20387, Feb. 2025, https://doi.org/10.48084/etasr.9662.

[9] M. G. M. Abdolrasol *et al.*, "Artificial Neural Networks Based Optimization Techniques: A Review," *Electronics*, vol. 10, no. 21, Jan. 2021, Art. no. 2689, https://doi.org/10.3390/electronics10212689.

[10] P. Singh and J. S. Lather, "Artificial neural network-based dynamic power management of a DC microgrid: a hardware-in-loop real-time verification," *International Journal of Ambient Energy*, vol. 43, no. 1, pp. 1730–1738, Dec. 2022, https://doi.org/10.1080/01430750.2020.1720811.

[11] A. Joshi, S. Capezza, A. Alhaji, and M. Y. Chow, "Survey on AI and Machine Learning Techniques for Microgrid Energy Management Systems," *IEEE/CAA Journal of Automatica Sinica*, vol. 10, no. 7, pp. 1513–1529, Jul. 2023, https://doi.org/10.1109/JAS.2023.123657.

[12] C. Xia and C. Zhang, "Power Management Strategy of Hybrid Electric Vehicles Based on Quadratic Performance Index," *Energies*, vol. 8, no. 11, pp. 12458–12473, Nov. 2015, https://doi.org/10.3390/en81112325.

[13] J. Faraji, A. Ketabi, H. Hashemi-Dezaki, M. Shafie-Khah, and J. P. S. Catalão, "Optimal Day-Ahead Self-Scheduling and Operation of Prosumer Microgrids Using Hybrid Machine Learning-Based Weather and Load Forecasting," *IEEE Access*, vol. 8, pp. 157284–157305, 2020, https://doi.org/10.1109/ACCESS.2020.3019562.

[14] M. M. Alam, M. H. Rahman, M. F. Ahmed, M. Z. Chowdhury, and Y. M. Jang, "Deep learning based optimal energy management for photovoltaic and battery energy storage integrated home micro-grid system," *Scientific Reports*, vol. 12, no. 1, Sep. 2022, Art. no. 15133, https://doi.org/10.1038/s41598-022-19147-y.

[15] L. Lv, X. Fang, S. Zhang, X. Ma, and Y. Liu, "Optimization of grid-connected voltage support technology and intelligent control strategies for new energy stations based on deep learning," *Energy Informatics*, vol. 7, no. 1, Aug. 2024, Art. no. 73, https://doi.org/10.1186/s42162-024-00382-8.

[16] B. Chandrasekar *et al.*, "Non-Isolated High-Gain Triple Port DC–DC Buck-Boost Converter With Positive Output Voltage for Photovoltaic Applications," *IEEE Access*, vol. 8, pp. 113649–113666, 2020, https://doi.org/10.1109/ACCESS.2020.3003192.

[17] B. Azeri, K. Javanmardi, S. Sofimowloodi, A. Attar, and A. Amini, "Utilizing Deep Learning Techniques to Eliminate the Current Sensor in a Boost Converter Used in a DC Nano-Grid," in *2024 31st International Conference on Mixed Design of Integrated Circuits and System (MIXDES)*, Gdansk, Poland, Jun. 2024, pp. 241–246, https://doi.org/10.23919/MIXDES62605.2024.10613968.

[18] G. Say, S. H. Hosseini, and P. Esmaili, "Hybrid Source Multi-Port Quasi-Z-Source Converter with Fuzzy-Logic-Based Energy Management," *Energies*, vol. 16, no. 12, Jan. 2023, Art. no. 4801, https://doi.org/10.3390/en16124801.

[19] M. Pushpavalli and N. M. Jothi Swaroopan, "KY converter with fuzzy logic controller for hybrid renewable photovoltaic/wind power system," *Transactions on Emerging Telecommunications Technologies*, vol. 31, no. 12, Dec. 2020, Art. no. e3989, https://doi.org/10.1002/ett.3989.

[20] D. Valencia, N. Pozo, and A. Sanchez, "Multi-Variable Fuzzy+PID Control of a Buck-Boost Four Port Converter for Renewable Energy System," in *2022 IEEE International Autumn Meeting on Power, Electronics and Computing (ROPEC)*, Ixtapa, Mexico, Nov. 2022, pp. 1–6, https://doi.org/10.1109/ROPEC55836.2022.10018676.

[21] R. Ostadian, J. Ramoul, A. Biswas, and A. Emadi, "Intelligent Energy Management Systems for Electrified Vehicles: Current Status, Challenges, and Emerging Trends," *IEEE Open Journal of Vehicular Technology*, vol. 1, pp. 279–295, 2020, https://doi.org/10.1109/OJVT.2020.3018146.

[22] M. Vijayan *et al.*, "Optimal PI-Controller-Based Hybrid Energy Storage System in DC Microgrid," *Sustainability*, vol. 14, no. 22, Jan. 2022, Art. no. 14666, https://doi.org/10.3390/su142214666.